Data on Global Change (Carbon Dioxide Information Analysis Center, Oak Ridge National Laboratory, U.S. Department of Energy, Oak Ridge, TN, 2002).
27. C. Goyet, P. G. Poisson, *Deep-Sea Res.* **36**, 2635 (1989).
28. We used the dissociation constants derived from (*27*) to calculate the equilibrium DIC concentration. Using different constants resulted in negligible changes in our estimates.
29. The preformed alkalinity distribution is essential because it largely determines the oceanic buffer capacity. Preformed alkalinity was derived using a multiple linear regression of the surface (<60 dbar) alkalinity distribution for each of the three ocean basins in a way similar to the technique used by Sabine *et al.* (*12*). Using in situ alkalinity instead of preformed alkalinity resulted in negligible changes in our results.
30. Our method requires the oceanic biological carbon pump to be in a preindustrial steady state. Anthropogenic CO_2 is assumed to be a perturbation propagating through the ocean as a tracer inert to the biological carbon pump.
31. Most models suggest that the CO_2 air-sea disequilibrium has been increasing with time (*16*). However, the extent of this increase varies between models. This bias is reduced by estimating anthopogenic CO_2 on shorter time scales (such as decadal) during which the disequilibrium is closer to constant than over longer time scales (since preindustrial times).
32. R. J. Matear, A. C. Hirst, *Tellus* **51B**, 722 (1999).
33. The global oceanic inventory of anthropogenic CO_2 from 1980 to 1989 and from 1990 to 1999 was calculated on a 1° grid at 100 m intervals and integrated to 5000 m for the Atlantic and 2000 m for the Indian and Pacific Oceans. The objective mapping techniques used were based on the methods described by Sarmiento *et al.* (*38*). For the basinwide inventories, the Southern Ocean was split from 120°E to 70°W for the Pacific, 70°W to 30°E for the Atlantic, and 30°E to 120°E for the Indian Ocean. Aside from the Southern Ocean, the major continents were taken to be main boundaries separating the ocean basins.
34. We used the OGCM to estimate the combined bias and uncertainty of our anthropogenic CO_2 uptake estimates by comparing the simulated and estimated inventory from CFC predictions in the model. Our model analysis suggests that the CFC age technique is biased ~8% lower (30.1 Pg of C) than the total simulated anthropogenic CO_2 inventory from 1980 to 1999 (32.8 Pg of C). We are hesitant to apply this "correction" because there is good agreement between our CFC age–based inventory and those using the direct techniques (MLR and isopycnal) in the Indian Ocean (Fig. 1), which suggests that the model bias may be exaggerated. Instead, we expand our estimated uncertainty to ~15%, which includes both the predicted "bias" from our model analysis (including mixing and disequilibrium) and the uncertainty in the inventories obtained from the MLR and isopycnal analyses. The measurement precision of CFC was taken to be ±0.005 pmol/kg. Adding this value to the simulated CFCs in the model resulted in an uncertainty of about 5% in the global inventory. Repeat measurements of CFCs show differences in CFC ages from year to year (*39*). As model simulations may underestimate interannual variability in the ocean, we added extra "noise" to the CFC measurements in the model (±0.01 pmol/kg), which resulted in a further 10% uncertainty in our estimates. The uncertainty associated with the inventory calculation was determined using two different interpolation schemes (objective and loess) and was estimated to be 2%. The total uncertainty of our estimate (~20%) was calculated by a sum-of-squares propagation of all uncertainties with the assumption that each is independent of the others. We believe the uncertainty of our estimates to be an upper limit, given the good consistency between our estimated inventory in the Indian Ocean and those using the direct methods (*10*, *12*) (Fig. 1). Because these direct techniques (MLR and isopycnal) are not subject to the uncertainties associated with the CFC age method (for example, in ages and disequilibrium), they provide evidence of upper-bound errors.
35. The predicted warming of the ocean in the climate change simulation (0.3°C) was in good agreement with observations from 1950 to 1998 (*40*) and provides confidence that the model is simulating recent changes in the ocean.
36. To simulate anthropogenic CO_2 uptake, models use constant climate and assume that biological processes are operating in a steady state. These are the same assumptions used for the CFC age technique.
37. J. C. Orr *et al.*, paper presented at the International Geosphere-Biosphere Programme Open Science Conference, Amsterdam, 10 to 13 July 2001. For more details and to download the results of this study, go to www.ipsl.jussieu.fr/OCMIP/.
38. J. L. Sarmiento, J. Willebrand, S. Hellerman, *Objective Analysis of Tritium Observations in the Atlantic Ocean During 1971–1974* (Ocean Tracer Laboratory Tech Report 1, Princeton Univ. Press, Princeton, NJ, 1982).
39. S. C. Doney, J. L. Bullister, R. Wanninkhof, *Geophys. Res. Lett.*, **25**, 1399 (1998).
40. S. Levitus, J. I. Antonov, T. P. Boyer, C. Stephens, *Science* **287**, 2225 (2000).

41. This study would not have been possible without the efforts of those responsible for collecting and analyzing CFCs during WOCE and making those measurements available. They include R. Fine, M. Rhein, W. Roether, W. Smethie, M. Warner, Y. Watanabe, R. Weiss, and C. S. Wong. We also thank three anonymous reviewers and C. Sweeney for comments on the text. B.I.B. and R.M.K. were supported by NSF (grants OCE9819144 and OCE9986310), J.L.B. was supported by NOAA's Office of Global Programs and Global Carbon Cycle Program, J.L.S. was supported by the Carbon Modeling Consortium, and R.J.M. was supported by Environment Australia and the CSIRO Climate Change Program.

16 August 2002; accepted 20 November 2002

Satellite Observations of Magnetic Fields Due to Ocean Tidal Flow

Robert H. Tyler,[1]* Stefan Maus,[2] Hermann Lühr[2]

The ocean is an electrically conducting fluid that generates secondary magnetic fields as it flows through Earth's main magnetic field. Extracting ocean flow signals from remote observations has become possible with the current generation of satellites measuring Earth's magnetic field. Here, we consider the magnetic fields generated by the ocean lunar semidiurnal (M_2) tide and demonstrate that magnetic fields of oceanic origin can be clearly identified in satellite observations.

In a fully magnetohydrodynamic process, the flow and electromagnetic fields are coupled. In the ocean, however, flow generates electromagnetic fields but the electromagnetic fields are not thought to affect the flow appreciably. This reduced magnetohydrodynamic case is often called "motional induction" and can be understood as follows. The dissolved salts in seawater form hydrated, electrically charged ions. As the charged ions are carried by the ocean flow through Earth's main magnetic field, they are deflected by the Lorentz force, which acts in a direction perpendicular to both the velocity and magnetic field. This leads to various combinations of two effects. First, the migrating ions can accumulate to form electrical spatial charge densities that in turn create electric fields that tend to prevent further migration of charge. Second, the spatial charge densities can be relieved by electrical shorting through surrounding sections of the water or electrically conducting sediments. The latter effect involves electrical currents and the associated secondary magnetic fields, which are the subject of this paper.

Two components of the ocean-generated magnetic field can be distinguished. The first is a "toroidal" component that has been estimated to reach maximum amplitudes of 100 nT but is confined to the ocean and sediments and is therefore not observable remotely (*1*–*5*). This component results from electric current circuits closing in planes containing the vertical axis. The second is a much weaker (1 to 10 nT) "poloidal" component with large spatial decay scales that allow the magnetic fields to reach remote land and satellite locations (*4*, *6*–*10*). This component involves electric current circuits closing horizontally and is the least understood because it is generated by large-scale integrals of ocean flow transport and estimates typically require large-domain integrations.

But this dependence of the far-reaching poloidal magnetic fields on transport integrals also makes these fields attractive. In principle, information about past and present ocean variability is contained in the land and satellite magnetic records, and this variability would primarily reflect integrated transport quantities (including in ice-covered regions) that are difficult to obtain using other methods (*11*). Understanding such ocean variability is a key factor in addressing climate and global change concerns, and although an assessment of the potential for exploiting the magnetic fields in this way is beyond the scope of this paper, here we describe

[1]Ocean Physics Department, Applied Physics Laboratory, University of Washington, 1013 NE 40th Street, Seattle, WA 98103, USA. [2]GeoForschungsZentrum (GFZ), Telegrafenberg, 14473 Potsdam, Germany.

*To whom correspondence should be addressed. E-mail: tyler@apl.washington.edu

an initial step in identifying ocean flow effects in the satellite record. We have performed a global numerical prediction of the magnetic fields due to the semidiurnal M_2 ocean tidal constituent and have compared it with observations made aboard the CHAMP (Challenging Minisatellite Payload) satellite, and we found close agreement between the observations and predictions.

In the numerical prediction, the tidal flow and main magnetic field used are given by the results (TPXO.5.1) of Egbert (*12*) and the CO2 model (*13*), respectively. The model formulation is based on a thin-sheet induction equation [similar to the formulation discussed first by Price (*14*) but with several modifications made for the case of ocean flow forcing (*15*)] coupled to equations describing zero-laplacian magnetic potentials outside the shell (*16*). Independent of the prediction, the periodic M_2 magnetic-field variations were extracted from CHAMP satellite measurements collected over 2 years (*16*). Figure 1 displays their real and imaginary parts against the corresponding model predictions (see also movie S1). A comparison of their spectra over ocean and land (Fig. 2) confirms that the observed M_2 signal is stronger over the ocean.

The predicted and observed ocean-generated magnetic fields agree remarkably well. The long bands of enhanced amplitude (yellow and blue stripes in Fig. 1) running across all longitudes are very much the same in the observation and the model results. A closer inspection reveals that even regional peaks (red or dark blue spots) can be found to match in most cases. Meridional stripes, visible in Fig. 1C for the Pacific Ocean, are probably a line-leveling problem due to incompletely removed magnetospheric fields. An assimilation of the data into the model could remove this effect, but we regarded a completely independent treatment of measurements and model as important for this first test. In rare cases, weak anomaly centers appear unrealistically over the source-free land areas. This is an effect of the along-track filtering (applied to both model and observed data), which transports signal from the ocean onto the land areas. Another effect of filtering is to reduce the local amplitude peaks of the predicted signal, which at satellite altitude reached 3 nT before filtering. Both of these filtering effects are illustrated in fig. S1.

As a check for potential systematic differences in the amplitudes, Fig. 3 shows the amplitudes of the observed and the predicted signals averaged over latitude and plotted against longitude. Apart from the aforementioned line-leveling problem (the short-scale oscillations with longitude), the curves track each other closely both in shape and amplitude despite the fact that the predictions were calculated assuming an insulating mantle. This model assumption was initially made to provide an upper-bound estimate while avoiding somewhat ad hoc assumptions regarding the mantle conductivity structure. We anticipated that the predictions would systematically overestimate the longer wavelengths due to the absence of coupling with the lower mantle. Though mantle effects at some level are both expected and possibly evident in our results, a discussion of this does not appear to be required for the primary purposes of this paper and is postponed.

Focusing on the lunar M_2 tide, it has been shown here for the first time that the ocean

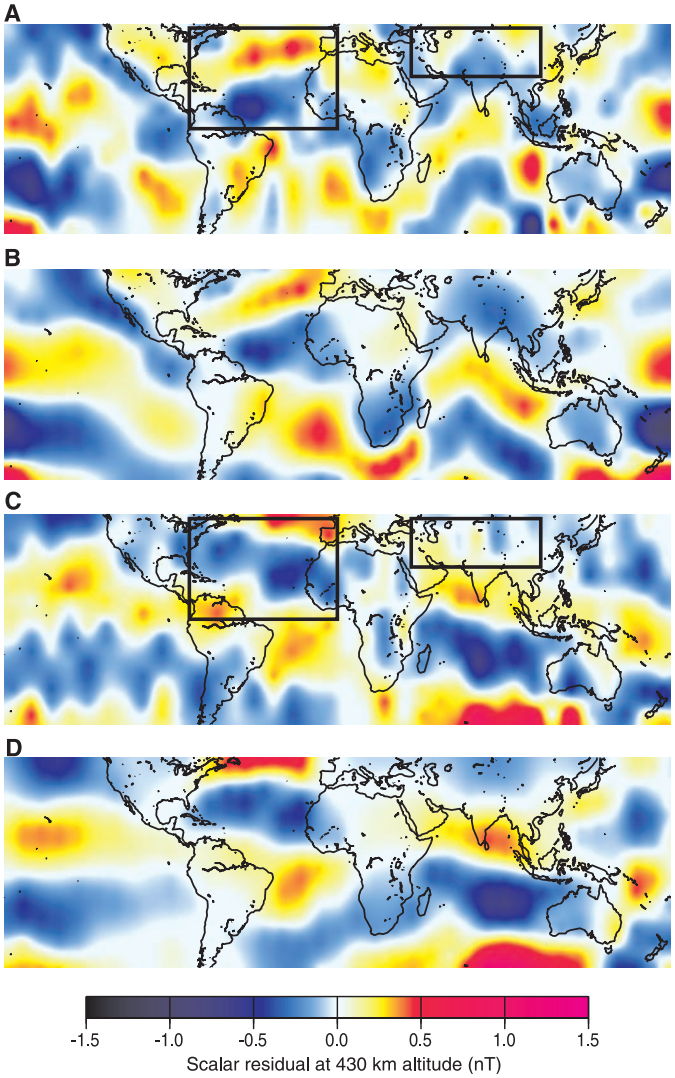

Fig. 1. Predicted and observed magnetic signal (scalar anomaly) of the M_2 ocean tide. Along-track filtering to remove large-scale (>10,000 km) magnetospheric fields has been applied to both. Representing the periodic signal in terms of its real component M_r (phase = 0°) and its imaginary component M_i (phase = 90°), the observations are displayed in (**A**) and (**C**) against the corresponding predictions in (**B**) and (**D**) (see also movie S1). The rectangles in (A) and (C) indicate the areas from which the spectra of Fig. 2 were computed.

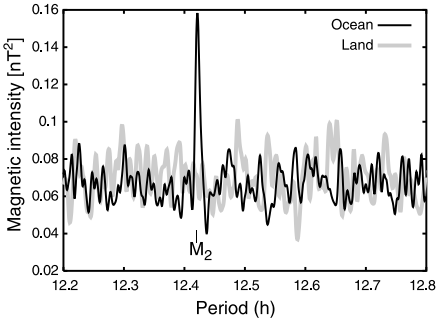

Fig. 2. Magnetic intensity spectra of the data from the areas indicated in Fig. 1. Although the ocean area exhibits a clear M_2 peak, this is absent from the land data.

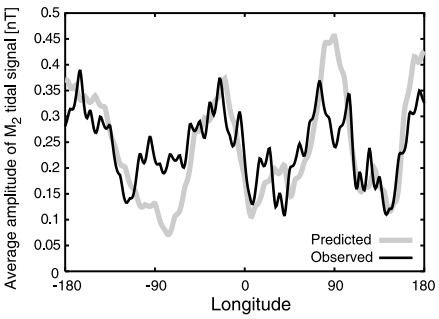

Fig. 3. Meridionally averaged magnetic signal amplitude. Predicted and observed amplitudes are almost congruent. In two regions there are, however, obvious deviations. Around –90° longitude, the model underestimates the tidal signal. This longitude maps to the Gulf of Mexico but also to the west coast of South America. Conversely, the model predicts too large a signal in the Indian Ocean (90° longitude).

flow makes a substantial contribution to the geomagnetic field at satellite altitude. This has important implications: In broader terms, it encourages future studies to assess the feasibility of monitoring ocean flow from space. A more immediate consequence, however, is that it shows that oceanic signals must be incorporated into geomagnetic field models. Indeed, with recent advances in internal and external field separation (*17*), the ocean flow signal is now the strongest remaining signal in the low-latitude magnetic residuals that has not yet been modeled. Correcting magnetic readings for ocean flow signals could strongly improve the accuracy of lithospheric anomaly maps and greatly raise the detectability of small-scale crustal magnetization.

References and Notes

1. T. B. Sanford, *J. Geophys. Res.* **76**, 3476 (1971).
2. A. D. Chave, D. S. Luther, *J. Geophys. Res.* **95**, 7185 (1990).
3. R. H. Tyler, L. A. Mysak, *Geophys. Astrophys. Fluid Dyn.* **80**, 167 (1995).
4. R. H. Tyler, L. A. Mysak, J. M. Oberhuber, *J. Geophys. Res.* **102**, 5531 (1997).
5. F. E. M. Lilley, J. H. Filloux, P. J. Mulhearn, I. J. Ferguson, *J. Geomagn. Geoelectr.* **45**, 403 (1993).
6. J. C. Larsen, *Geophys. J. R. Astron. Soc.* **16**, 47 (1968).
7. S. R. C. Malin, *Geophys. J. R. Astron. Soc.* **21**, 447 (1970).
8. N. L. Bindoff, F. E. M. Lilley, J. H. Filloux, *J. Geomagn. Geoelectr.* **40**, 1445 (1988).
9. J. D. McKnight, *Geophys. J. Int.* **122**, 889 (1995).
10. R. H. Tyler, T. B. Sanford, J. M. Oberhuber, *J. Geomagn. Geoelectr.* **49**, 1351 (1997).
11. R. H. Tyler, thesis, McGill University (1995).
12. G. D. Egbert, A. F. Bennet, M. G. G. Foreman, *J. Geophys. Res.* **99**, 24821 (1994).
13. R. Holme, N. Olsen, M. Rother, H. Lühr, in *First CHAMP Mission Results for Gravity, Magnetic and Atmospheric Studies*, C. Reigber. H. Lühr, P. Schwintzer, Eds. (Springer, Berlin, in press).
14. A. T. Price, *Q. J. Mech. Appl. Math.* **2**, 283 (1949).
15. R. H. Tyler, paper presented at the Third International Conference on Marine Electromagnetics, Stockholm, 11 to 13 July 2001.
16. Materials and methods are available as supporting material on *Science* Online.
17. S. Maus *et al.*, *Geophys. Res. Lett.* **29**, 10.1029/2001GL013685 (2002).

18. CHAMP is supported by Deutsches Zentrum für Luft- und Raumfahrtechnik under contract FKZ 50 EP 9587, data analyses were supported by Deutsche Forschungsgemeinschaft (SPP 1097), and the numerical prediction results are based on work supported by NASA (under award NAG5-10570) and the Office of Naval Research (under award N00014-99-1-0407).

Supporting Online Material

www.sciencemag.org/cgi/content/full/299/5604/239/DC1
Materials and Methods
Fig. S1
Movie S1

4 September 2002; accepted 8 November 2002

Dispersal, Environment, and Floristic Variation of Western Amazonian Forests

Hanna Tuomisto,[1]* Kalle Ruokolainen,[1] Markku Yli-Halla[2]

The distribution of plant species, the species compositions of different sites, and the factors that affect them in tropical rain forests are not well understood. The main hypotheses are that species composition is either (i) uniform over large areas, (ii) random but spatially autocorrelated because of dispersal limitation, or (iii) patchy and environmentally determined. Here we test these hypotheses, using a large data set from western Amazonia. The uniformity hypothesis gains no support, but the other hypotheses do. Environmental determinism explains a larger proportion of the variation in floristic differences between sites than does dispersal limitation; together, these processes explain 70 to 75% of the variation. Consequently, it is important that management planning for conservation and resource use take into account both habitat heterogeneity and biogeographic differences.

Unraveling the relative importance of biological interactions, random variation, dispersal limitation, and environmental determinism in creating differences in species composition among sites (beta diversity) is a central issue in plant ecology (*1*–*7*). The hypothesis that the plant species composition of Amazonian noninundated forests is uniform over large areas emphasizes the role of biological interactions: It is suggested that the forests are dominated by a limited suite of competitively superior tree species (*8*, *9*). The hypothesis that plant species composition fluctuates in a random walk emphasizes dispersal history: The species are competitively equal, and floristic differences are created through random but spatially limited dispersal of species that evolved in different areas (*2*, *10*, *11*). The hypothesis that species distributions are patchy emphasizes environmental determinism: The forests are considered to be a mosaic where plant species composition is determined by edaphic and other environmental site characteristics (*12*, *13*). Which of these hypotheses is accepted as the main explanatory model has important practical implications for biodiversity conservation, forest management, and the planning and interpretation of ecological research.

To test how well the distributions of Amazonian plant species conform to the three hypotheses, we inventoried 163 sites in four regions in western Amazonia (Colombia, Ecuador, northern Peru, and southern Peru) using a standard quantitative procedure (500-m–by–5-m line transects) (*14*, *15*). The inventories included noninundated forests on clay or loam soils (122 sites; henceforth called tierra firme) and on white sand soils (3 sites) and seasonally inundated and swamp forests (38 sites). The topography of the transects ranged from flat to hilly (with a difference in elevation of up to 60 m), depending on local terrain. We inventoried two distinct plant groups: pteridophytes (ferns and fern allies) and the Melastomataceae (a family of shrubs and small trees). Because these groups are both phylogenetically remote and dispersed by different agents (wind versus animals), they provide independent test cases for measuring the relative importance of processes related to evolution, dispersal limitation, biological interactions, and niche differentiation. By focusing on these plant groups, we were able to compare voucher specimens and apply a uniform taxonomy over all regions; hence, we did not need to exclude unnamed morphospecies from the analyses [as is usually done in tree inventories (*8*, *9*, *11*)]. Our approach also yields relatively high numbers of individuals per species and an indication of leveling-off of the species-area curve within each site (*13*, *14*), which should dampen the effect of sampling error. The data set includes 286 species and 297,000 individuals of pteridophytes, and 265 species and 40,300 individuals of Melastomataceae. We analyzed several (usually three) composite soil samples from each site (*15*) to obtain quantitative data on mean soil chemistry and texture (tables S1 and S2).

We first examined the hypothesis that tierra firme forests are uniform over wide areas, especially when only the most abundant species are considered (*8*, *9*). If the forests are uniform, then floristic similarity among sites should be uniformly high and have no identifiable pattern; in particular, the degree of floristic similarity should not depend on the geographic distance between sites or on differences in their environmental conditions. We tested these predictions with Mantel tests, and they were refuted for both pteridophytes and Melastomataceae: Floristic distance between sites showed a significant correlation with both environmental and geographic distance (Table 1). These correlations were

[1]Department of Biology, University of Turku, FIN-20014 Turku, Finland. [2]MTT Agrifood Research Finland, FIN-31600 Jokioinen, Finland.

*To whom correspondence should be addressed. E-mail: hantuo@utu.fi.